An integral method for numerical simulation of MRI artifacts induced by metallic implants

S. Balac[1], G. Caloz[1], G. Cathelineau[2],
B. Chauvel[2] and J.D. de Certaines[3]

[1] Institut de Recherche Mathématique de Rennes,
UMR CNRS 6625, Université de Rennes 1, France

[2] Laboratoire de Biomatériaux en Site Osseux,
Université de Rennes 1, France

[3] Laboratoire de Résonance Magnétique en Biologie et Médecine,
Université de Rennes 1, France

Short title: Numerical simulation of MRI susceptibility artifacts

Correspondence:
Prof. Gabriel Caloz
Institut de Recherche Mathématique de Rennes
Campus de Beaulieu
35042 RENNES cedex
France

Tel: 33 2 99 28 60 53
fax : 33 2 99 28 67 90
email : Gabriel.Caloz@univ-rennes1.fr

Abstract

Numerical simulation is a valuable tool for the study of magnetic susceptibility artifacts from metallic implants. A major difficulty in the simulation lies in the computation of the magnetic field induced by the metallic implant. A new method has been designed and implemented to compute the magnetic field induced by metallic objects of arbitrary shape. The magnetic field is expressed pointwise in terms of a surface integral. Efficient quadrature schemes are proposed to evaluate this integral. Finally, the method is linked to an artifact reconstruction model to simulate the images.

Key words: susceptibility artifacts, numerical simulation, magnetic field computation

1 Introduction

In magnetic resonance imaging (MRI) even minor perturbations of the gradients can disturb the imaging process and may render the clinical image inaccurate or useless. Common causes of magnetic field perturbation are changes of magnetic properties in the sample like metallic implanted objects, such as dental prosthesis, orthopedic apparatus, *etc.* Metallic surgical instruments used in interventional MRI are also responsible for magnetic field perturbation. In the case of guided stereotactic surgery, image distortions are especially harmful since geometrical accuracy is required.

In the past, several studies involving numerical simulation have been undertaken to help in the understanding and to establish experimental conditions that determine susceptibility artifacts, see [1], [2], [3] for instance. However, these simulation attempts have been restricted to simple test objects (cylinders, spheres or ellipsoids) for which an analytical expression for the induced magnetic field is known. In general, a precise calculation of the magnetic field involves a boundary value problem with partial differential equations (PDE) derived from Maxwell's equations and requires the use of PDE approximation schemes. Among the classical numerical methods are the finite element method (FEM), the finite difference method (FDM) and the boundary element method (BEM). For a comprehensive treatment of these numerical methods in electromagnetism we refer to [4]. Our approach, which is based on a surface integral representation formula for the magnetic flux density, is most similar to the BEM. In short, our method consists of expressing the problem in an integral form over the boundary of the implant and dividing the boundary into elements in which the integral is numerically computed. It is able to deal with objects of any shape provided that a mesh of the object boundary is available. This requirement is not at all restricting since mesh generation tools are widely used in computer assisted design (CAD). The advantages of our method compared to the FEM [5] or to the FDM [6] are numerous. First, the computation depends only on the object boundary so that the discretization of space is reduced from 3D to 2D. Furthermore, in the FDM/FEM the exterior domain must be truncated

and an approximation of the behavior of the field at infinity must be introduced on an artificial boundary. With the BEM, the behavior at infinity is always exactly satisfied. Finally, for 3D problems the FEM and the FDM lead to large linear systems to be solved, whereas in the proposed method the solution is obtained pointwise by evaluating a surface integral.

In the current work, this magnetic field computation method has been linked to artifact reconstruction algorithms ([1], [3]) to generate simulated images of MRI susceptibility artifacts from paramagnetic metallic implants. Our algorithm could also be used in conjunction with the computer simulation program for MRI imaging sequences described in [7]. Among the applications of a MRI susceptibility artifacts simulation computer program are the systematic investigation of artifact behavior under various experimental conditions. It may also be very useful in the design of new medical implants compatible with MRI. Implant properties can be easily modified by changing parameters in the software.

2 Mathematical modeling

Let Ω be the domain filled by the metallic implant and Σ be its boundary, see figure 1. The exterior domain $\Omega_e = \mathbb{R}^3 \backslash \Omega$ is assumed to be a homogeneous medium having negligible magnetization (we assume that the metallic implant has magnetic properties which are very different from the surrounding tissues). We only consider the effect of the main static magnetic flux $\mathbf{B_0}$ and neglect the effect of the exciting RF pulses. In this study, the metallic implant is supposed to be an isotropic linear paramagnetic material and its magnetization $\mathbf{M}$ is assumed to be uniform and parallel to the applied field,

$$\mathbf{M} = \frac{\chi_\mathbf{m}}{\mu_\mathbf{0}} \mathbf{B_0}, \tag{1}$$

where χ_m is the magnetic susceptibility of the material. One has to point out that for ferromagnetic materials, constitutive laws for the magnetization are non linear and the mathematical model is much more difficult to handle. However, patients bearing ferromagnetic implants are restricted from being examined by MRI.

In term of magnetic flux density $\mathbf{B_i} = \mathbf{B} - \mathbf{B_0}$ the problem, deduced from Maxwell's equations, is

$$\begin{cases} \text{div } \mathbf{B_i} &= 0 \text{ in } \mathbb{R}^3, \\ \text{curl } \mathbf{B_i} &= 0 \text{ in } \Omega \text{ and } \Omega_e, \\ \left[\mathbf{B_i} \wedge \mathbf{n}\right] &= \mu_0 \left(\mathbf{M} \wedge \mathbf{n}\right) \text{ at the interface } \Sigma, \end{cases} \tag{2}$$

with the condition at infinity $\lim_{P \to \infty} \mathbf{B_i}(\mathbf{P}) = \mathbf{0}$. In equations (2), $\mathbf{n}$ is the unit outward normal to Σ and $[\cdot]$ denotes the jump across the boundary Σ. One can prove (see [10]) that the solution $\mathbf{B_i}$ of problem (2) can

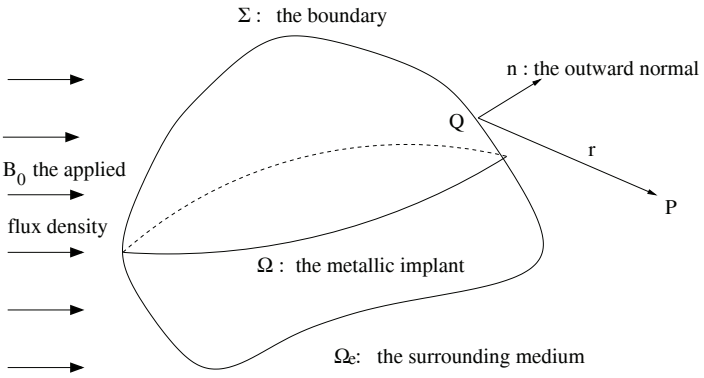

Figure 1: Studied Configuration

be expressed as

$$\mathbf{B_i}(\mathbf{P}) = \mu_0 \ \delta_\Omega(\mathbf{P}) \ \mathbf{M} + \frac{\mu_0}{4\pi} \iint_{\Sigma} \left(\mathbf{M} \cdot \frac{\mathbf{r}}{\mathbf{r^3}}\right) \ \mathbf{n}(\mathbf{Q}) \ \mathrm{ds}(\mathbf{Q}), \tag{3}$$

where $\mathbf{r} = \mathbf{QP}$ and $\delta_\Omega(P) = 1$ if $P \in \Omega$ and 0 otherwise.

Therefore, the magnetic flux density $\mathbf{B_i}$ in P is obtained by computing the integral

$$\mathcal{I}(P) = \iint_{\Sigma} \left(\mathbf{M} \cdot \frac{\mathbf{r}}{\mathbf{r^3}}\right) \ \mathbf{n}(\mathbf{Q}) \ \mathrm{ds}(\mathbf{Q}). \tag{4}$$

3 Method and computations

3.1 Computational method

We assume that the boundary Σ is modeled as a finite union of flat and curved triangles, see figures 2 and 3. Let T_h^1 denote the set of all flat triangles and T_h^2 the set of all curved triangles. Then the integral in (3) can be decomposed into two terms

$$\mathcal{I}(P) = \sum_{K \in T_h^1} \iint_K \left(\mathbf{M} \cdot \frac{\mathbf{r}}{\mathbf{r^3}}\right) \ \mathbf{n}(\mathbf{Q}) \ \ \mathrm{ds}(\mathbf{Q}) + \sum_{\mathbf{K} \in \mathbf{T_h^2}} \iint_{\mathbf{K}} \left(\mathbf{M} \cdot \frac{\mathbf{r}}{\mathbf{r^3}}\right) \ \mathbf{n}(\mathbf{Q}) \ \mathrm{ds}(\mathbf{Q}). \tag{5}$$

In order to improve the accuracy of the method, these two sums noted $S_1(P)$ and $S_2(P)$ are evaluated in two distinct ways.

For flat triangles, the normal $\mathbf{n}$ to Σ is constant on each triangle and we can express $S_1(P)$ as

$$S_1(P) = \sum_{K \in T_h^1} \left(\mathbf{M} \cdot \iint_{\mathbf{K}} \frac{\mathbf{r}}{\mathbf{r^3}} \ \ \mathrm{ds}(\mathbf{Q})\right) \mathbf{n} \ . \tag{6}$$

Consequently to evaluate $S_1(P)$, one has to compute the integral of $\mathbf{r}/r^3$ over a set of triangles. Such an

integral can be calculated exactly, see for instance [8] or [9] for the resulting formulae. This result is of great practical importance since for the flat parts of the object boundary no numerical scheme (and therefore no approximation) is needed to evaluate $S_1(P)$. Besides, it is important to notice that for any polyhedral object, the induced magnetic field can therefore be calculated exactly.

To evaluate $S_2(P)$, the integral over each curved triangle is computed by using a Gaussian quadrature rule. It has to be noted that the computation of $S_2(P)$ by a quadrature method is hampered by the singular behavior of the function $\mathbf{M} \cdot \mathbf{r}/r^3$ when the point P is very close to the boundary Σ. However this difficulty can be overcome by using an adaptative integration scheme (see [10]).

A full presentation of the way the integrals are calculated and a precise discussion of the numerical accuracy of the method may be found in [10]. The source code is public domain and can be obtained from the authors.

3.2 Numerical simulation

To demonstrate the accuracy of the method, results of the numerical computation have been verified against analytic calculations for a 2 cm diameter titanium ball (its magnetic susceptibility is $\chi_m = 2\ 10^{-4}$) and a magnetic flux density $\mathbf{B_0}$ of 0.5 T. Figure 2 shows the mesh of the ball surface (680 triangles) and the isolines for the component of the induced magnetic flux $\mathbf{B_i}$ along $\mathbf{B_0}$, in a slice parallel to the magnetic flux density $\mathbf{B_0}$ passing through the center of the ball. The magnetic field has been computed for 128×128 points in the slice. The maximal pointwise relative error does not exceed 0.05%. Computations have been done on a `Sun Enterprise 450` and have required 184 seconds.

The magnetic field computation method has been linked to an artifact reconstruction algorithm to illustrate its efficiency. We have used the algorithm described in ([1], [3]) that focuses on geometric distorsions (distorsions of the slice and distorsions in the read-out gradient direction) due to perturbations of the magnetic field gradients, see [11] p. 209. We present some simulations carried out with a dental implant depicted in figure 3. This implant had a magnetic susceptibility of 10^{-3} usi and was placed in a 0.5 T magnetic flux density $\mathbf{B_0}$. The mesh of the implant boundary used to compute the magnetic field perturbation had 1328 triangles (we have neglected the thread of the screw). The magnetic field has been computed for 128×128 points in the slice depicted in figure 3. The slice had a side length of 5 cm and was parallel to the magnetic flux density $\mathbf{B_0}$. Computations have required 224 seconds. Figure 4 shows the isolines for the component of $\mathbf{B_i}$ along $\mathbf{B_0}$. From the magnetic field values the computed image in figure 5 has been obtained by the above mentioned image reconstruction algorithm. To obtain the corresponding experimental image the implant was placed centrally in a box filled with a diamagnetic substance ($CuSO_4$ at a concentration of 0.6 g/l). The

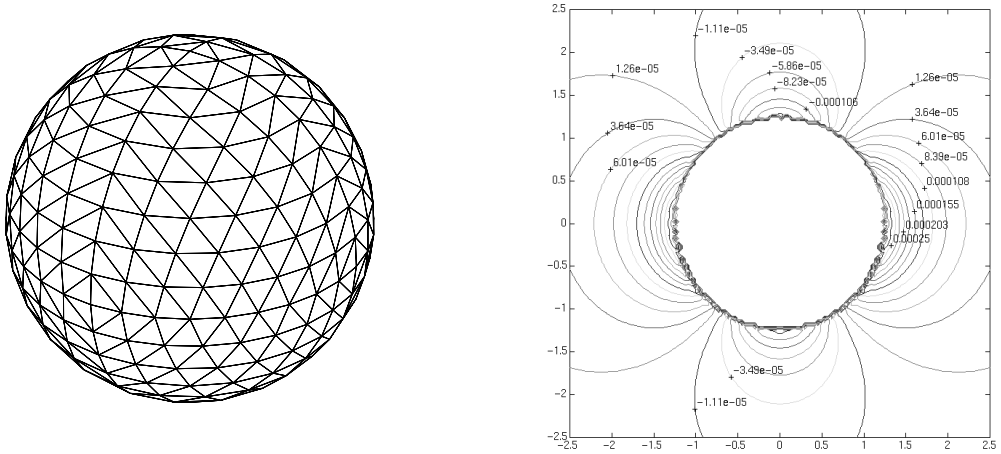

Figure 2: Mesh of the sphere (680 triangles) and isolines for the component of $\mathbf{B_i}$ along $\mathbf{B_0}$.

slice was recorded using a spin-echo sequence with a repetition time of 490 ms and an echo time of 25 ms. The slice-selection gradient and the read-out gradient strength were 10^{-2} T/m. The slice thickness was 3 mm.

4 Discussion

The numerical experiments indicate that the magnetic field computation method is very accurate and fast. This is of great importance since the results are to be linked to the image reconstruction procedure to obtain the simulated images of susceptibility artifacts in MRI. These requirements would not be fully fulfilled by standard numerical methods.

We obtained numerically simulated MRI susceptibility artifacts from the magnetic field computations using the artifact reconstruction procedure described in ([1], [3]). This procedure only takes into account geometric distortions due to perturbations of the magnetic field gradients by the induced magnetic field. Therefore comparison between numerically simulated and experimental MRI images should concern the image structure rather than absolute pixel value. We refer to [7] for some further developments in the direction of sequence simulation.

Although we have restricted ourselves to magnetic susceptibility artifacts, there are other artifacts due to metallic object, such as RF-induced eddy currents, see ([12], [13]).

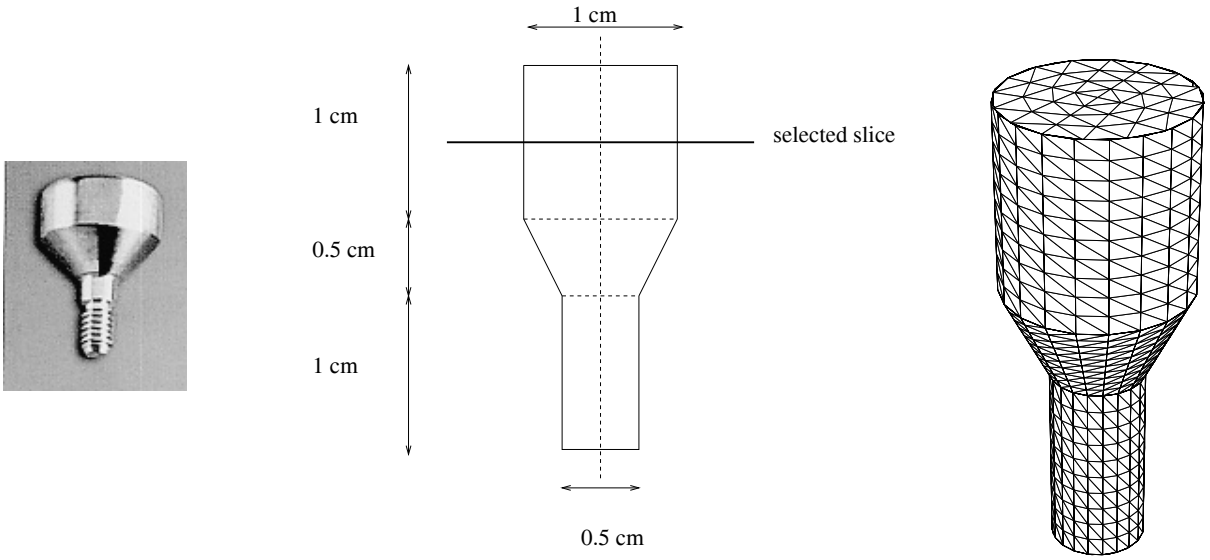

Figure 3: Dental implant chosen to illustrate the effectiveness of the method, position of the slice and mesh (1328 triangles) of the implant boundary used to compute the magnetic field perturbation.

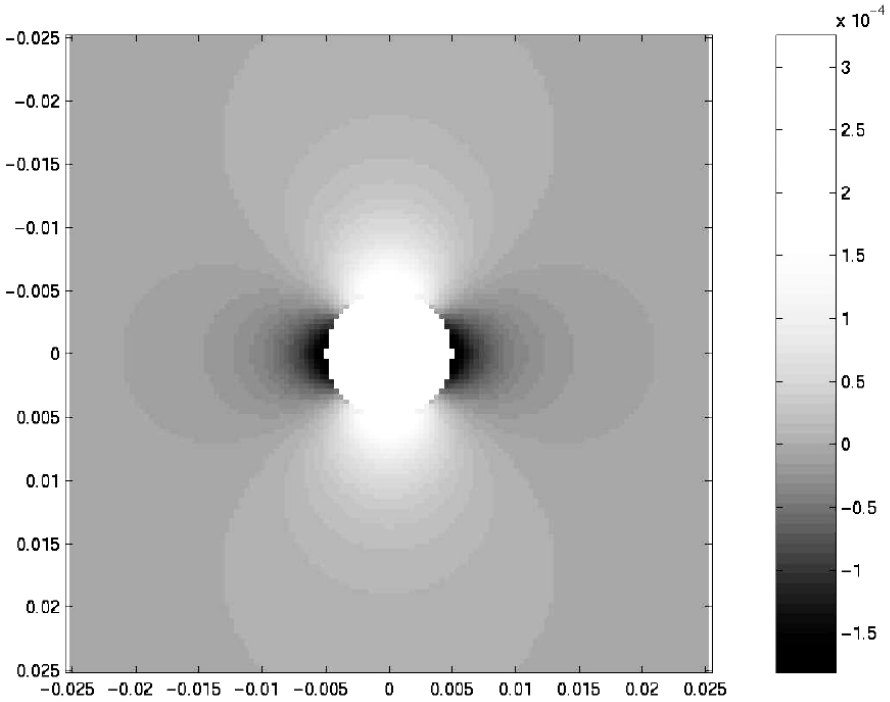

Figure 4: isolines for the component of $\mathbf{B_i}$ along $\mathbf{B_0}$. Field values range from $-1.5\ 10^{-4}$ to $3\ 10^{-4}$ Tesla.

A 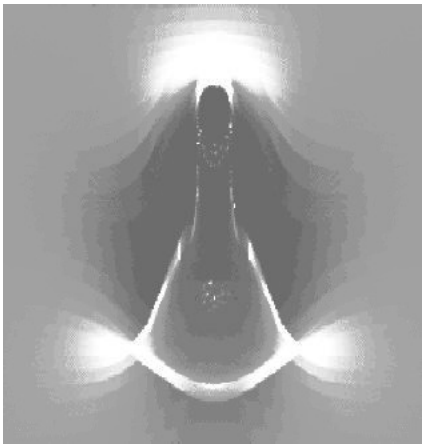 B 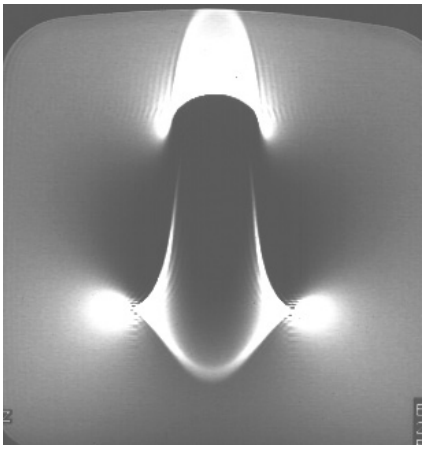

Figure 5: (A) simulated spin-echo image - (B) experimental MRI image (SE 490/25). The frequency encoding gradient direction is left-right, the width of the figures corresponds to 5 cm actual distance.

5 Conclusion

An original numerical technique has been presented for computing the magnetic field induced by a metallic object. The advantages of the present approach are its simplicity and its computational efficiency. The method has been combined with artifact reconstruction algorithms ([1], [3]) to simulate susceptibility artifacts in MRI. It could also be used in conjunction with other simulation programs [7]. The various applications for a method of accurately predicting susceptibility artifacts include facilitating the design of new medical implants that are not as likely to cause image distortions. Currently, designers must construct and image numerous prototypes in order to test new ideas. Further work includes combining the current method with an algorithm for predicting the artifacts resulting from eddy currents induced by RF fields or field gradients.

References

[1] K. M. Ludeke, P. Roschmann, R. Tischler, Susceptibility artifacts in NMR imaging. *Magn. Reson. Imaging* **3**, 329–343, (1985).

[2] J.F. Schenck, The role of magnetic susceptibility in magnetic resonance imaging. *Med. Phys.* **23**, 815–850, (1996).

[3] A. Erricsson, A. Hemmingsson, B. Jung, G. O. Sperber, Calculation of MRI artefacts caused by static field disturbances. *Phys. Med. Biol.* **33**:1103, (1988).

[4] M. Sadiku, "Numerical techniques in electromagnetism", CRC Press, 1992.

[5] S. Li, G. Williams, T. Frisk, B. Arnold, M. Smith, A computer simulation of the static magnetic field distribution in the human head. *Magn. Reson. Med.*, **34**, 268-275, (1995).

[6] R. Bhagwandien, M.A. Moerland, C.J.G. Bakker, R. Beersma, J.J.W. Lagendijk, Numerical analysis of the magnetic field for arbitrary magnetic susceptibility distributions in 3D. *Magn. reson. Imaging* **12**, 101–107, (1994).

[7] M. Olsson, R. Wirestam, B. Persson, A computer simulation program for MR imaging: application to RF and static magnetic field imperfections. *Magn. Reson. Med.*, **34**, 612-617, (1995).

[8] S. Balac, G. Caloz, Magnetic susceptibility artifacts in magnetic resonance imaging: calculation of the magnetic field disturbances. *IEEE Trans. Magn.* **32** 1645–1648, (1996).

[9] Z. Ren, F. Bouillault, A. Razek, J.C. Vérité, An efficient semi-analytical integration procedure in three dimensional boundary integral method. *COMPEL* **7**, 195–205, (1988).

[10] S. Balac, G. Caloz, Induced magnetic field computations using a boundary integral formulation. *Report 2-99, Dept of mathematics, University of Brest, France,* (1999).

[11] P. Callaghan, "Principles of nuclear magnetic resonance microscopy", Clarendon Press, 1993.

[12] C.R. Camacho, D.B. Plewes, R.M. Henkelman, Nonsusceptibility artifacts due to metallic objects in MR imaging. *JMRI* **5**, 75–88, (1995).

[13] L. Bennett, P. Wang, M. Donahue, Artifacts in magnetic resonance imaging from metals. *J. Appl. Phys.* **79**, 4712–4714, (1996).

[14] B. Chauvel, G. Cathelineau, S. Balac, J. Lecerf, J.D. de Certaines, Cancellation of metal induced MRI artifacts with dual component paramagnetic and diamagnetic material: mathematical modelization and experimental verification. *JMRI* **6**, 936–938, (1996).